*J. Fluid Mech.* (2023), *vol*. 955, A15, doi:10.1017/jfm.2022.1072

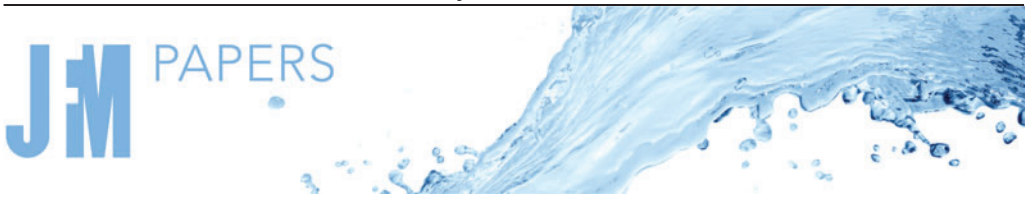


# Strain self-amplification is larger than vortex stretching due to an invariant relation of filtered velocity gradients

**P.-F. Yang[1,2], Z.D. Zhou[1,2], H. Xu[3] and G.W. He[1,2,†]**

[1]State Key Laboratory of Nonlinear Mechanics, Institute of Mechanics, Chinese Academy of Sciences, Beijing 100190, PR China

[2]School of Engineering Sciences, University of Chinese Academy of Sciences, Beijing 100049, PR China

[3]Center for Combustion Energy and School of Aerospace Engineering, Tsinghua University, Beijing 100084, PR China

(Received 30 July 2022; revised 15 October 2022; accepted 8 December 2022)

A relation among invariants of filtered velocity gradients with two different filter sizes is derived. Based on this relation and physical reasoning, it is shown analytically that strain self-amplification contributes more to energy transfer than vortex stretching in homogeneous turbulence, as observed in recent numerical investigations of homogeneous isotropic turbulence. We note that the invariant relation studied and hence the inequality between strain self-amplification and vortex stretching apply to all homogeneous flows, not restricted to isotropic turbulence.

**Key words:** homogeneous turbulence, turbulence theory

## 1. Introduction

Turbulence is a nonlinear, multi-scale and dissipative system. In three-dimensional turbulent flows, the energy is injected at large scales, gradually transfers to smaller scales and ultimately dissipates at the smallest scales of the system. This energy cascade picture was first phenomenologically introduced by Richardson (1922) and later developed theoretically by Kolmogorov, which led to the celebrated K41 theory (Kolmogorov 1941*a*,*b*). Nowadays, energy cascade is regarded as one of the hallmarks of turbulence and has been widely discussed in the literature (Tennekes & Lumley 1972; Frisch 1995; Pope 2000; Davidson 2015; He, Jin & Yang 2017). Among studies of energy cascade, an insightful approach is to discuss the properties of the filtered velocity gradient tensor (FVGT) (Borue & Orszag 1998; Tao, Katz & Meneveau 2000, 2002; van der Bos *et al.* 2002; Higgins, Parlange & Meneveau 2003; Leung, Swaminathan

† Email address for correspondence: hgw@lnm.imech.ac.cn

& DaVidson 2012; Fiscaletti *et al.* 2016*a*,*b*; Danish & Meneveau 2018; Johnson 2021), as FVGTs are closely related to velocity increments (Eyink 1995) and represent flow motion at filter scales. Specifically, the symmetric and antisymmetric parts of the velocity gradient, that is, the strain rate and vorticity, represent the deformation and the rotation of the fluid parcel, respectively. A long-standing concept in turbulence dynamics is that vortex stretching (VS) drives the energy cascade (Taylor 1937, 1938; Tennekes & Lumley 1972; Pullin & Saffman 1998; Davidson 2015; Doan *et al.* 2018). Recently, the self-amplification of straining motion has been proposed as an alternative mechanism of energy cascade (Tsinober 2009; Carbone & Bragg 2020; Johnson 2020, 2021). In particular, by studying the energy transfer term in the Kármán–Howarth equation, Carbone & Bragg (2020) provided evidence that strain self-amplification (SSA) dominates over VS in energy cascade. Johnson (2020) derived an exact relation between the subgrid-scale (SGS) stress tensor and the FVGT, which was then used to numerically evaluate the contributions of VS and SSA to the energy cascade and led to the conclusion that SSA is larger than VS. These important observations give us new insights into turbulent inter-scale energy transfer. In this paper, we first obtain a relation for the invariants of FVGTs with two different filtered sizes, which could be regarded as a generalization of the Betchov relation for the velocity gradient tensor (Betchov 1956) to scales beyond the dissipative range. Then we use this relation to demonstrate analytically that SSA contributes more to energy cascade than VS. Data from direct numerical simulation (DNS) of homogeneous isotropic turbulence (HIT) are used to confirm our theoretical reasoning. We note that our derivations require only homogeneity, but not isotropy, and thus can be applied to any homogeneous flows, not only HIT.

## 2. Relation for invariants of FVGTs in homogeneous turbulence

We start with the relation for the invariants of the velocity gradient tensor $A_{ij} \equiv \partial u_i/\partial x_j$, where $\boldsymbol{u}(\boldsymbol{x}, t)$ is the velocity field. We use the symbol $\bar{y}^\ell$ to denote the low-pass filtering operation to any field $y(\boldsymbol{x})$:

$$\bar{y}^\ell(\boldsymbol{x}) = \int_V \mathscr{G}^\ell(\boldsymbol{r}) y(\boldsymbol{x}+\boldsymbol{r})\,\mathrm{d}\boldsymbol{r}, \tag{2.1}$$

where $\mathscr{G}^\ell(\boldsymbol{r})$ is the filter defined on the domain $V$. In this work, we choose the widely used Gaussian filter with $V = \mathbb{R}^3$:

$$\mathscr{G}^\ell(\boldsymbol{r}) = \frac{1}{(2\pi\ell^2)^{3/2}}\,\mathrm{e}^{-|\boldsymbol{r}|^2/2\ell^2}, \tag{2.2}$$

which, when applied to a field, would retain spatial variations with scale larger than $\sim \ell$ but suppress those with scale smaller than $\sim \ell$. Thus $\bar{u}_i^\ell$ and $\bar{A}_{ij}^\ell \equiv \partial \bar{u}_i^\ell/\partial x_j$ refer respectively to the velocity and FVGT filtered by a Gaussian filter with size $\ell$. We restrict our discussion to incompressible flows; thus $A_{ii} = \bar{A}_{ii}^\ell = 0$. Note that a second-rank tensor can always be decomposed into its symmetric and antisymmetric parts: $A_{ij} = S_{ij} + \Omega_{ij}$, where $S_{ij} \equiv (A_{ij} + A_{ji})/2$ and $\Omega_{ij} \equiv (A_{ij} - A_{ji})/2$. Similarly we define $\bar{S}_{ij}^\ell$ and $\bar{\Omega}_{ij}^\ell$, with $\bar{A}_{ij}^\ell = \bar{S}_{ij}^\ell + \bar{\Omega}_{ij}^\ell$.

Betchov (1956) proved two relations for the invariants of $A_{ij}$ in homogeneous and incompressible flows:

$$\langle A_{ij}A_{ji}\rangle = \langle A_{ij}A_{jk}A_{ki}\rangle = 0, \tag{2.3}$$

where the brackets $\langle\ \rangle$ denote the ensemble average. Equation (2.3) can be expressed in terms of $S_{ij}$ and $\Omega_{ij}$:

$$\langle S_{ij}S_{ji}\rangle = -\langle \Omega_{ij}\Omega_{ji}\rangle = \tfrac{1}{2}\langle \omega_i\omega_i\rangle, \tag{2.4}$$

$$\langle S_{ij}S_{jk}S_{ki}\rangle = -3\langle \Omega_{ij}S_{jk}\Omega_{ki}\rangle = -\tfrac{3}{4}\langle \omega_i S_{ij}\omega_j\rangle, \tag{2.5}$$

where $\omega_i = -\epsilon_{ijk}\Omega_{jk}$ is the vorticity vector and $\epsilon_{ijk}$ is the permutation tensor. Equation (2.4) connects the amplitudes of vorticity and the rate of strain, while (2.5), remarkably, relates the mean rate of VS $\langle \omega_i S_{ij}\omega_j\rangle$ to the third-order moments of strain $\langle S_{ij}S_{jk}S_{ki}\rangle$, which provides further insight into the statistics of $A_{ij}$ (Meneveau 2011). On the other hand, using FVGT allows us to investigate the interactions between strain and vorticity with different filtered sizes (Leung *et al.* 2012; Fiscaletti *et al.* 2016*b*; Lozano-Durán, Holzner & Jiménez 2016), for which (2.3) needs to be extended. To that end, we note that recently Yang *et al.* (2022) derived a general relation for the invariants involving three vector gradient fields $\partial a_i/\partial x_j$, $\partial b_i/\partial x_j$ and $\partial c_i/\partial x_j$ in homogeneous flows:

$$\begin{aligned}\left\langle \frac{\partial a_i}{\partial x_j}\frac{\partial b_j}{\partial x_k}\frac{\partial c_k}{\partial x_i}\right\rangle + \left\langle \frac{\partial a_i}{\partial x_j}\frac{\partial c_j}{\partial x_k}\frac{\partial b_k}{\partial x_i}\right\rangle = \left\langle \frac{\partial a_i}{\partial x_j}\frac{\partial b_j}{\partial x_i}\frac{\partial c_k}{\partial x_k}\right\rangle + \left\langle \frac{\partial b_i}{\partial x_j}\frac{\partial c_j}{\partial x_i}\frac{\partial a_k}{\partial x_k}\right\rangle \\ + \left\langle \frac{\partial c_i}{\partial x_j}\frac{\partial a_j}{\partial x_i}\frac{\partial b_k}{\partial x_k}\right\rangle - \left\langle \frac{\partial a_i}{\partial x_i}\frac{\partial b_j}{\partial x_j}\frac{\partial c_k}{\partial x_k}\right\rangle.\end{aligned} \tag{2.6}$$

Note that the derivation of the above only used the chain rule of derivatives and homogeneity. Special cases of (2.6) were known before. For example, Appendix D of Eyink (2006) discussed the case when $a_i$, $b_i$ and $c_i$ are all solenoidal, and Yang, Pumir & Xu (2020) derived the form for $a_i = b_i = c_i$ but without requiring zero divergence. Now if we choose the fields $a_i$ and $b_i$ to be the filtered velocity with filter size $\ell_1$ and $c_i$ to be the filtered velocity with a different filter size $\ell_2$, i.e. $a_i = b_i = \bar{u}_i^{\ell_1}$ and $c_i = \bar{u}_i^{\ell_2}$, (2.6) gives

$$\langle \bar{A}_{ik}^{\ell_1}\bar{A}_{kj}^{\ell_1}\bar{A}_{ji}^{\ell_2}\rangle = 0, \tag{2.7}$$

which can be further expressed as

$$\begin{aligned}\langle \bar{A}_{ik}^{\ell_1}\bar{A}_{kj}^{\ell_1}\bar{A}_{ji}^{\ell_2}\rangle &= \langle (\bar{S}_{ik}^{\ell_1} + \bar{\Omega}_{ik}^{\ell_1})(\bar{S}_{kj}^{\ell_1} + \bar{\Omega}_{kj}^{\ell_1})(\bar{S}_{ji}^{\ell_2} + \bar{\Omega}_{ji}^{\ell_2})\rangle \\ &= \langle \bar{S}_{ik}^{\ell_1}\bar{S}_{kj}^{\ell_1}\bar{S}_{ji}^{\ell_2}\rangle + \langle \bar{\Omega}_{ik}^{\ell_1}\bar{\Omega}_{kj}^{\ell_1}\bar{S}_{ji}^{\ell_2}\rangle + 2\langle \bar{\Omega}_{ik}^{\ell_1}\bar{S}_{kj}^{\ell_1}\bar{\Omega}_{ji}^{\ell_2}\rangle = 0.\end{aligned} \tag{2.8}$$

Physically, we can regard $\langle \bar{S}_{ik}^{\ell_1}\bar{S}_{kj}^{\ell_1}\bar{S}_{ji}^{\ell_2}\rangle$ as the interaction between strain at scale $\ell_1$ and strain at scale $\ell_2$, $\langle \bar{\Omega}_{ik}^{\ell_1}\bar{\Omega}_{kj}^{\ell_1}\bar{S}_{ji}^{\ell_2}\rangle$ as the vorticity at scale $\ell_1$ stretched by the strain at scale $\ell_2$ and $\langle \bar{\Omega}_{ik}^{\ell_1}\bar{S}_{kj}^{\ell_1}\bar{\Omega}_{ji}^{\ell_2}\rangle$ as the interaction between strain and vorticity at scale $\ell_1$ with vorticity at scale $\ell_2$. In the next section we show that those terms in (2.8) are closely related to the SSA and VS mechanisms defined in Johnson (2020), and based on (2.8) one can show that SSA contributes more to inter-scale energy transfer than VS.

## 3. The SSA is larger than VS

By filtering the Navier–Stokes equation, one can readily obtain the evolution equation for the filtered velocity $\bar{u}_i^{\ell}$:

$$\frac{\partial \bar{u}_i^{\ell}}{\partial t} + \bar{u}_j^{\ell}\frac{\partial \bar{u}_i^{\ell}}{\partial x_j} = -\frac{\partial \bar{p}^{\ell}}{\partial x_i} + \nu\nabla^2\bar{u}_i^{\ell} + \bar{f}_i^{\ell} - \frac{\partial \tau_{ij}^{\ell}}{\partial x_j}, \tag{3.1}$$

where $\tau_{ij}^{\ell} \equiv \overline{u_i u_j}^{\ell} - \bar{u}_i^{\ell}\bar{u}_j^{\ell}$ refers to the SGS stress tensor. Multiplying (3.1) with $\bar{u}_i^{\ell}$ yields the equation for the large-scale kinetic energy $\frac{1}{2}\bar{u}_i^{\ell}\bar{u}_i^{\ell}$:

$$\frac{\partial \frac{1}{2}\bar{u}_i^{\ell}\bar{u}_i^{\ell}}{\partial t} + \frac{\partial \Phi_j^{\ell}}{\partial x_j} = \bar{u}_i^{\ell}\bar{f}_i^{\ell} - \Pi^{\ell} - 2\nu\bar{S}_{ij}^{\ell}\bar{S}_{ij}^{\ell}, \tag{3.2}$$

where $\Phi_j^{\ell}$ is a flux term (cf. (2.20*b*) of Johnson 2021) whose contribution vanishes in homogeneous flows and $\Pi^{\ell} \equiv -\tau_{ij}^{\ell}\bar{S}_{ij}^{\ell}$ is the energy transfer term discussed extensively in the literature (Meneveau & Katz 2000; Ballouz & Ouellette 2018, 2020; Buzzicotti *et al.* 2018; Dong *et al.* 2020; Vela-Martín & Jiménez 2021). Johnson (2020) showed that for the Gaussian filter (equation (2.2)), the SGS stress tensor $\tau_{ij}^{\ell}$ is related to the FVGT $\bar{A}_{ij}^{\ell}$ via

$$\tau_{ij}^{\ell} = \int_0^{\ell^2} \mathrm{d}\theta \overline{\bar{A}_{ik}^{\sqrt{\theta}}\bar{A}_{jk}^{\sqrt{\theta}}}^{\sqrt{\ell^2-\theta}}, \tag{3.3}$$

which helps us analyse the energy transfer term $\Pi^{\ell}$ in the filtered energy equation (3.2). Plugging (3.3) into the definition of $\Pi^{\ell}$ yields

$$\begin{aligned}
\Pi^{\ell} = -\tau_{ij}^{\ell}\bar{S}_{ij}^{\ell} &= -\int_0^{\ell^2} \mathrm{d}\theta \overline{\bar{A}_{ik}^{\sqrt{\theta}}\bar{A}_{jk}^{\sqrt{\theta}}}^{\sqrt{\ell^2-\theta}}\bar{S}_{ij}^{\ell} \\
&= \underbrace{-\int_0^{\ell^2} \mathrm{d}\theta \overline{\bar{S}_{ik}^{\sqrt{\theta}}\bar{S}_{jk}^{\sqrt{\theta}}}^{\sqrt{\ell^2-\theta}}\bar{S}_{ij}^{\ell}}_{\Pi_S^{\ell}} + \underbrace{\int_0^{\ell^2} \mathrm{d}\theta \overline{\bar{\Omega}_{ik}^{\sqrt{\theta}}\bar{\Omega}_{kj}^{\sqrt{\theta}}}^{\sqrt{\ell^2-\theta}}\bar{S}_{ij}^{\ell}}_{\Pi_{\Omega}^{\ell}} \\
&\quad + \underbrace{2\int_0^{\ell^2} \mathrm{d}\theta \overline{\bar{S}_{ik}^{\sqrt{\theta}}\bar{\Omega}_{kj}^{\sqrt{\theta}}}^{\sqrt{\ell^2-\theta}}\bar{S}_{ij}^{\ell}}_{\Pi_c^{\ell}},
\end{aligned} \tag{3.4}$$

where $\Pi_S^{\ell}$, $\Pi_{\Omega}^{\ell}$ and $\Pi_c^{\ell}$ correspond to the contributions to the inter-scale energy transfer due to the interaction of strain at scale $\ell$ respectively with strain, vorticity and the correlation between strain and vorticity at a scale smaller than or equal to $\ell$ (Johnson 2020). Direct numerical simulation results of Johnson (2020) showed that $\langle\Pi_S^{\ell}\rangle : \langle\Pi_{\Omega}^{\ell}\rangle : \langle\Pi_c^{\ell}\rangle \approx 5:3:0$ in the inertial range, which led to an important observation that the contribution of SSA to the energy transfer is larger than that of VS. Next we show that this observation can be justified analytically based on (2.8).

We start from the expression of $\langle\Pi^{\ell}\rangle$:

$$\begin{aligned}
\langle\Pi^{\ell}\rangle &= -\int_0^{\ell^2} \mathrm{d}\theta \langle\overline{\bar{A}_{ik}^{\sqrt{\theta}}\bar{A}_{jk}^{\sqrt{\theta}}}^{\sqrt{\ell^2-\theta}}\bar{S}_{ij}^{\ell}\rangle \\
&= -\int_0^{\ell^2} \mathrm{d}\theta \int_V \mathrm{d}\boldsymbol{r}\mathscr{G}^{\sqrt{\ell^2-\theta}}(\boldsymbol{r})\langle\bar{A}_{ik}^{\sqrt{\theta}}\bar{A}_{jk}^{\sqrt{\theta}}(\boldsymbol{x}+\boldsymbol{r})\bar{S}_{ij}^{\ell}(\boldsymbol{x})\rangle
\end{aligned}$$

$$= -\int_0^{\ell^2} \mathrm{d}\theta \int_V \mathrm{d}\boldsymbol{r}\mathscr{G}^{\sqrt{\ell^2-\theta}}(\boldsymbol{r})\langle \bar{A}_{ik}^{\sqrt{\theta}}\bar{A}_{jk}^{\sqrt{\theta}}(\boldsymbol{x})\bar{S}_{ij}^{\ell}(\boldsymbol{x}-\boldsymbol{r})\rangle$$

$$= -\int_0^{\ell^2} \mathrm{d}\theta \langle \bar{A}_{ik}^{\sqrt{\theta}}\bar{A}_{jk}^{\sqrt{\theta}}\overline{\bar{S}^{\ell}}_{ij}^{\sqrt{\ell^2-\theta}}\rangle = -\int_0^{\ell^2} \mathrm{d}\theta \langle \bar{A}_{ik}^{\sqrt{\theta}}\bar{A}_{jk}^{\sqrt{\theta}}\bar{S}_{ij}^{\sqrt{2\ell^2-\theta}}\rangle, \tag{3.5}$$

where the third equality holds due to homogeneity and the last equality comes from the property of the Gaussian filter: $\overline{\bar{y}^{\alpha}}^{\beta} = \bar{y}^{\sqrt{\alpha^2+\beta^2}}$ (e.g. Pope 2000, p. 567). Applying the approach of (3.5) to those terms on the right-hand side of the second equality in (3.4), one can easily obtain that

$$\langle \Pi_S^{\ell}\rangle = \int_0^{\ell^2} \mathrm{d}\theta(-\langle \bar{S}_{ik}^{\sqrt{\theta}}\bar{S}_{kj}^{\sqrt{\theta}}\bar{S}_{ji}^{\sqrt{2\ell^2-\theta}}\rangle), \tag{3.6}$$

$$\langle \Pi_{\Omega}^{\ell}\rangle = \int_0^{\ell^2} \mathrm{d}\theta\langle \bar{\Omega}_{ik}^{\sqrt{\theta}}\bar{\Omega}_{kj}^{\sqrt{\theta}}\bar{S}_{ji}^{\sqrt{2\ell^2-\theta}}\rangle, \tag{3.7}$$

$$\langle \Pi_c^{\ell}\rangle = 2\int_0^{\ell^2} \mathrm{d}\theta\langle \bar{S}_{ik}^{\sqrt{\theta}}\bar{\Omega}_{kj}^{\sqrt{\theta}}\bar{S}_{ji}^{\sqrt{2\ell^2-\theta}}\rangle. \tag{3.8}$$

We note that these forms of expressions for $\langle \Pi_S^{\ell}\rangle$, $\langle \Pi_{\Omega}^{\ell}\rangle$ and $\langle \Pi_c^{\ell}\rangle$ have not been shown before. We should also recall that (3.6) to (3.8) can only be applied on average, while the expression given by Johnson (2020), i.e. (3.4), holds pointwise. Next, the integrand $\langle \bar{A}_{ik}^{\sqrt{\theta}}\bar{A}_{jk}^{\sqrt{\theta}}\bar{S}_{ij}^{\sqrt{2\ell^2-\theta}}\rangle$ in the last expression in (3.5) can be expressed as

$$\langle \bar{A}_{ik}^{\sqrt{\theta}}\bar{A}_{jk}^{\sqrt{\theta}}\bar{S}_{ij}^{\sqrt{2\ell^2-\theta}}\rangle = \langle(\bar{S}_{ik}^{\sqrt{\theta}} + \bar{\Omega}_{ik}^{\sqrt{\theta}})(\bar{S}_{kj}^{\sqrt{\theta}} - \bar{\Omega}_{kj}^{\sqrt{\theta}})\bar{S}_{ij}^{\sqrt{2\ell^2-\theta}}\rangle$$

$$= \langle \bar{S}_{ik}^{\sqrt{\theta}}\bar{S}_{kj}^{\sqrt{\theta}}\bar{S}_{ji}^{\sqrt{2\ell^2-\theta}}\rangle - \langle \bar{\Omega}_{ik}^{\sqrt{\theta}}\bar{\Omega}_{kj}^{\sqrt{\theta}}\bar{S}_{ji}^{\sqrt{2\ell^2-\theta}}\rangle - 2\langle \bar{S}_{ik}^{\sqrt{\theta}}\bar{\Omega}_{kj}^{\sqrt{\theta}}\bar{S}_{ji}^{\sqrt{2\ell^2-\theta}}\rangle. \tag{3.9}$$

Plugging (3.9) into (3.5) yields

$$\langle \Pi^{\ell}\rangle = \int_0^{\ell^2} \mathrm{d}\theta \underbrace{(-\langle \bar{S}_{ik}^{\sqrt{\theta}}\bar{S}_{kj}^{\sqrt{\theta}}\bar{S}_{ji}^{\sqrt{2\ell^2-\theta}}\rangle)}_{I_1(\theta)} + \int_0^{\ell^2} \mathrm{d}\theta \underbrace{\langle \bar{\Omega}_{ik}^{\sqrt{\theta}}\bar{\Omega}_{kj}^{\sqrt{\theta}}\bar{S}_{ji}^{\sqrt{2\ell^2-\theta}}\rangle}_{I_2(\theta)}$$

$$+ 2\int_0^{\ell^2} \mathrm{d}\theta \underbrace{\langle \bar{S}_{ik}^{\sqrt{\theta}}\bar{\Omega}_{kj}^{\sqrt{\theta}}\bar{S}_{ji}^{\sqrt{2\ell^2-\theta}}\rangle}_{I_3(\theta)} = \langle \Pi_S^{\ell}\rangle + \langle \Pi_{\Omega}^{\ell}\rangle + \langle \Pi_c^{\ell}\rangle. \tag{3.10}$$

For simplicity, we denote $I_1(\theta) \equiv -\langle \bar{S}_{ik}^{\sqrt{\theta}}\bar{S}_{kj}^{\sqrt{\theta}}\bar{S}_{ji}^{\sqrt{2\ell^2-\theta}}\rangle$, $I_2(\theta) \equiv \langle \bar{\Omega}_{ik}^{\sqrt{\theta}}\bar{\Omega}_{kj}^{\sqrt{\theta}}\bar{S}_{ji}^{\sqrt{2\ell^2-\theta}}\rangle$ and $I_3(\theta) \equiv \langle \bar{S}_{ik}^{\sqrt{\theta}}\bar{\Omega}_{kj}^{\sqrt{\theta}}\bar{S}_{ji}^{\sqrt{2\ell^2-\theta}}\rangle$. Since $0 \leqslant \theta \leqslant \ell^2$, we always have $\sqrt{\theta} \leqslant \sqrt{2\ell^2-\theta}$. Notice that $I_1$ and $I_2$ are just the first and second terms on the left-hand side of (2.8), with $\ell_1 = \sqrt{\theta} < \ell_2 = \sqrt{2\ell^2-\theta}$, and $I_3$ represents the energy transfer by the strain-rate tensor at larger scale $\sqrt{2\ell^2-\theta}$ acting on the correlation of strain rate and vorticity at smaller scale $\sqrt{\theta}$ (Johnson 2020). Thus choosing $\ell_1 = \sqrt{\theta}$ and $\ell_2 = \sqrt{2\ell^2-\theta}$ in (2.8)

yields

$$\underbrace{-\langle \bar{S}_{ik}^{\sqrt{\theta}} \bar{S}_{kj}^{\sqrt{\theta}} \bar{S}_{ji}^{\sqrt{2\ell^2-\theta}} \rangle}_{I_1(\theta)} = 2 \underbrace{\langle \bar{\Omega}_{ik}^{\sqrt{\theta}} \bar{S}_{kj}^{\sqrt{\theta}} \bar{\Omega}_{ji}^{\sqrt{2\ell^2-\theta}} \rangle}_{I_4(\theta)} + \underbrace{\langle \bar{\Omega}_{ik}^{\sqrt{\theta}} \bar{\Omega}_{kj}^{\sqrt{\theta}} \bar{S}_{ji}^{\sqrt{2\ell^2-\theta}} \rangle}_{I_2(\theta)}, \tag{3.11}$$

which, by denoting $I_4(\theta) \equiv \langle \bar{\Omega}_{ik}^{\sqrt{\theta}} \bar{S}_{kj}^{\sqrt{\theta}} \bar{\Omega}_{ji}^{\sqrt{2\ell^2-\theta}} \rangle$, is simply written as

$$I_1(\theta) = 2I_4(\theta) + I_2(\theta). \tag{3.12}$$

Therefore, as long as $I_4(\theta) > 0$, $I_1(\theta)$ will be greater than $I_2(\theta)$, and $\langle \Pi_S^\ell \rangle = \int_0^{\ell^2} I_1(\theta)\,\mathrm{d}\theta$ will be larger than $\langle \Pi_\Omega^\ell \rangle = \int_0^{\ell^2} I_2(\theta)\,\mathrm{d}\theta$.

Now we show that $I_4(\theta) > 0$ in homogeneous turbulence. Applying the properties of the Gaussian filter again we have

$$\begin{aligned} I_4(\theta) &= \langle \bar{\Omega}_{ik}^{\sqrt{\theta}} \bar{S}_{kj}^{\sqrt{\theta}} \bar{\Omega}_{ji}^{\sqrt{2\ell^2-\theta}} \rangle = \langle \bar{\Omega}_{ik}^{\sqrt{\theta}} \bar{S}_{kj}^{\sqrt{\theta}} \overline{\bar{\Omega}_{ji}^{\sqrt{\theta}}}^{\sqrt{2\ell^2-2\theta}} \rangle \\ &= \int_V \mathrm{d}\boldsymbol{r} \langle \bar{\Omega}_{ik}^{\sqrt{\theta}}(\boldsymbol{x}) \bar{S}_{kj}^{\sqrt{\theta}}(\boldsymbol{x}) \bar{\Omega}_{ji}^{\sqrt{\theta}}(\boldsymbol{x}+\boldsymbol{r}) \rangle \mathscr{G}^{\sqrt{2\ell^2-2\theta}}(\boldsymbol{r}) \\ &= \int_V \mathrm{d}\boldsymbol{r} G_4^{\sqrt{\theta}}(\boldsymbol{r}) \mathscr{G}^{\sqrt{2\ell^2-2\theta}}(\boldsymbol{r}), \end{aligned} \tag{3.13}$$

where we denoted $G_4^{\sqrt{\theta}}(\boldsymbol{r}) \equiv \langle \bar{\Omega}_{ik}^{\sqrt{\theta}}(\boldsymbol{x}) \bar{S}_{kj}^{\sqrt{\theta}}(\boldsymbol{x}) \bar{\Omega}_{ji}^{\sqrt{\theta}}(\boldsymbol{x}+\boldsymbol{r}) \rangle$ for simplicity. We first show that $\int_V \mathrm{d}\boldsymbol{r} G_4^{\sqrt{\theta}}(\boldsymbol{r}) = 0$ when $V$ is large enough:

$$\begin{aligned} \int_V \mathrm{d}\boldsymbol{r} G_4^{\sqrt{\theta}}(\boldsymbol{r}) &= \int_V \mathrm{d}\boldsymbol{r} \langle \bar{\Omega}_{ik}^{\sqrt{\theta}}(\boldsymbol{x}) \bar{S}_{kj}^{\sqrt{\theta}}(\boldsymbol{x}) \bar{\Omega}_{ji}^{\sqrt{\theta}}(\boldsymbol{x}+\boldsymbol{r}) \rangle \\ &= \int_V \mathrm{d}\boldsymbol{r} \left\langle \bar{\Omega}_{ik}^{\sqrt{\theta}}(\boldsymbol{x}) \bar{S}_{kj}^{\sqrt{\theta}}(\boldsymbol{x}) \frac{1}{2} \left( \frac{\partial \bar{u}_j^{\sqrt{\theta}}}{\partial x_i}(\boldsymbol{x}+\boldsymbol{r}) - \frac{\partial \bar{u}_i^{\sqrt{\theta}}}{\partial x_j}(\boldsymbol{x}+\boldsymbol{r}) \right) \right\rangle \\ &= \int_V \mathrm{d}\boldsymbol{r} \frac{1}{2} \left\langle \left( \bar{\Omega}_{jk}^{\sqrt{\theta}}(\boldsymbol{x}) \bar{S}_{ki}^{\sqrt{\theta}}(\boldsymbol{x}) - \bar{\Omega}_{ik}^{\sqrt{\theta}}(\boldsymbol{x}) \bar{S}_{kj}^{\sqrt{\theta}}(\boldsymbol{x}) \right) \frac{\partial \bar{u}_i^{\sqrt{\theta}}}{\partial x_j}(\boldsymbol{x}+\boldsymbol{r}) \right\rangle \\ &= \int_V \mathrm{d}\boldsymbol{r} \frac{1}{2} \frac{\partial}{\partial r_j} \langle (\bar{\Omega}_{jk}^{\sqrt{\theta}}(\boldsymbol{x}) \bar{S}_{ki}^{\sqrt{\theta}}(\boldsymbol{x}) - \bar{\Omega}_{ik}^{\sqrt{\theta}}(\boldsymbol{x}) \bar{S}_{kj}^{\sqrt{\theta}}(\boldsymbol{x})) \bar{u}_i^{\sqrt{\theta}}(\boldsymbol{x}+\boldsymbol{r}) \rangle \\ &= \int_V \mathrm{d}\boldsymbol{r} \frac{\partial}{\partial r_j} f_j(\boldsymbol{r}) = \oint_S ds_j f_j(\boldsymbol{r}) = 0, \end{aligned} \tag{3.14}$$

in which $f_j(\boldsymbol{r}) \equiv \langle \frac{1}{2} (\bar{\Omega}_{jk}^{\sqrt{\theta}}(\boldsymbol{x}) \bar{S}_{ki}^{\sqrt{\theta}}(\boldsymbol{x}) - \bar{\Omega}_{ik}^{\sqrt{\theta}}(\boldsymbol{x}) \bar{S}_{kj}^{\sqrt{\theta}}(\boldsymbol{x})) \bar{u}_i^{\sqrt{\theta}}(\boldsymbol{x}+\boldsymbol{r}) \rangle$, and we used the Gauss theorem with $S$ denoting the boundary of $V$ and $\boldsymbol{s}$ being the surface element of $S$. The last equality holds as long as $f_j(\boldsymbol{r})$ decreases fast enough when $|\boldsymbol{r}| \to \infty$, which is in general satisfied by any correlation function of a turbulent flow in an infinite space. For flows with periodic boundary conditions in space such as in most DNS, this simply requires that the simulation domain is large enough that the correlation decays sufficiently at the boundary.

A direct consequence of (3.14) is that $G_4^{\sqrt{\theta}}(\boldsymbol{r})$ must change sign over the domain $V$. As a correlation function between $\bar{\Omega}_{ik}^{\sqrt{\theta}}\bar{S}_{kj}^{\sqrt{\theta}}$ at position $\boldsymbol{x}$ and $\bar{\Omega}_{ji}^{\sqrt{\theta}}$ at position $\boldsymbol{x}+\boldsymbol{r}$, the sign change of $G_4^{\sqrt{\theta}}(\boldsymbol{r})$ corresponds to the change of the dominating interaction mechanism at the particular scale. For turbulence, when the separation $|\boldsymbol{r}|$ varies from the dissipative scale to the integral scale, the dynamics varies continuously from viscosity-dominated to inertia-dominated; thus a typical correlation function in turbulent flows should change sign at most once without the presence of another physical mechanism, as shown in figure 19.5 of Tritton (1988). Moreover, note that $G_4^{\sqrt{\theta}}(\boldsymbol{0}) = \langle \bar{\Omega}_{ik}^{\sqrt{\theta}}\bar{S}_{kj}^{\sqrt{\theta}}\bar{\Omega}_{ji}^{\sqrt{\theta}}\rangle$ is the filtered VS term and the net energy transfer from large to small scale in turbulence requires that $G_4^{\sqrt{\theta}}(\boldsymbol{0}) > 0$. Therefore, these two properties of $G_4^{\sqrt{\theta}}(\boldsymbol{r})$ means that $G_4^{\sqrt{\theta}}(\boldsymbol{r}) > 0$ in and only in a single-connected region $V_0$ enclosing the origin. Using these properties and that the Gaussian filter $\mathscr{G}^{\sqrt{2\ell^2-2\theta}}(\boldsymbol{r})$ in (3.13) is a monotonically decreasing function with $\boldsymbol{r}$, it is obvious that $\int_{V_0} \mathrm{d}\boldsymbol{r} G_4^{\sqrt{\theta}}(\boldsymbol{r})\ \mathscr{G}^{\sqrt{2\ell^2-2\theta}}(\boldsymbol{r}) > -\int_{V-V_0} \mathrm{d}\boldsymbol{r} G_4^{\sqrt{\theta}}(\boldsymbol{r})\mathscr{G}^{\sqrt{2\ell^2-2\theta}}(\boldsymbol{r})$, which yields $I_4(\theta) = \int_V \mathrm{d}\boldsymbol{r} G_4^{\sqrt{\theta}}(\boldsymbol{r})\ \mathscr{G}^{\sqrt{2\ell^2-2\theta}}(\boldsymbol{r}) > 0$. Then (3.12) gives that $\forall\theta \in [0, \ell^2]$, we have $I_1(\theta) > I_2(\theta)$, which easily leads to

$$\langle \Pi_S^\ell \rangle = \int_0^{\ell^2} I_1(\theta)\,\mathrm{d}\theta > \int_0^{\ell^2} I_2(\theta)\,\mathrm{d}\theta = \langle \Pi_\Omega^\ell \rangle. \tag{3.15}$$

In the next section we use DNS results to verify our discussions in this section.

## 4. Numerical results

The DNS of steady-state HIT is performed using a standard pseudo-spectral method on $N^3$ grids covering a periodic box of side $L = 2\pi$ (see Zhou, Wang & Jin (2018) and Zhou *et al.* (2019) for more details). In this work, three different cases with $N = 256$, 512 and 1024 were conducted, corresponding to the Taylor Reynolds number $R_\lambda = 129$, 206 and 302, respectively. Results reported below are mostly based on the data of $R_\lambda = 302$. Since we manipulate DNS of steady-state HIT, we use spatial and temporal averages to replace ensemble average. Statistics are collected from 100 snapshots equally spaced in $2T_E$ for the $R_\lambda = 206$ and 302 cases and 1200 snapshots in $21T_E$ for the $R_\lambda = 129$ case. Here $T_E = u'^2/\varepsilon$ denotes the eddy turnover time, where $u'$ is the root mean square of the turbulent fluctuating velocity and $\varepsilon$ is the dissipation rate. We also notice that in the derivation of the previous section, we assume the correlation decays fast enough when $|\boldsymbol{r}| \to \infty$. In the current DNS, as the simulation is constrained by the box size, we certainly could not let $|\boldsymbol{r}| \to \infty$, but the periodic condition ensures that the boundary integration on the left-hand side of the last equality of (3.14) vanishes, which guarantees that the assumptions in the theoretical derivation section are still satisfied by the current DNS. In addition, our theoretical demonstration could be applied to more general circumstances as long as the domain size is much larger than the integral scale of the flow.

In figure 1(*a*) we numerically check the integration relations derived in (3.10), i.e. $\langle \Pi_S^\ell \rangle = \int_0^{\ell^2} I_1(\theta)\,\mathrm{d}\theta$, $\langle \Pi_\Omega^\ell \rangle = \int_0^{\ell^2} I_2(\theta)\,\mathrm{d}\theta$ and $\langle \Pi_c^\ell \rangle = 2\int_0^{\ell^2} I_3(\theta)\,\mathrm{d}\theta$. In the figure, the symbols refer to $\langle \Pi_\Omega^\ell \rangle$, $\langle \Pi_S^\ell \rangle$ and $\langle \Pi_c^\ell \rangle$ calculated from their definitions (see (3.4)) and the solid lines are from the integrations of $I_1$, $I_2$ and $I_3$, all normalized by the dissipation rate $\varepsilon$ of the unfiltered flow field. These two approaches agree with each other within numerical precision, which verifies (3.10). In figure 1(*b*) we show the same quantity as in figure 1(*a*)

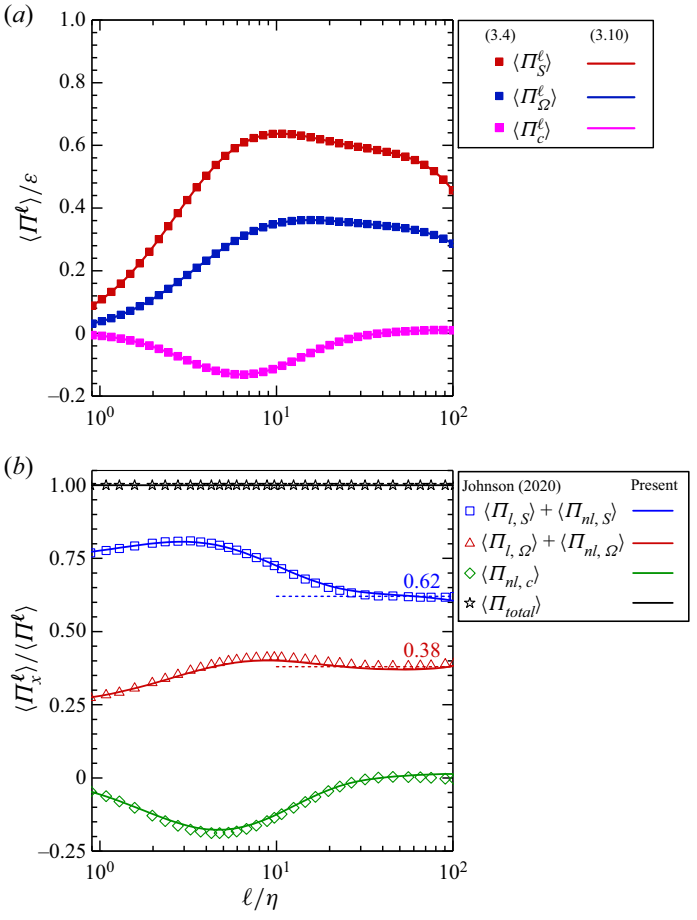


Figure 1. (*a*) Energy transfer terms calculated from their definitions, (3.4) (square symbols), and the corresponding integration expressions, (3.10) (solid lines). Red, blue and magenta colours refer to $\langle \Pi_S^\ell \rangle$, $\langle \Pi_\Omega^\ell \rangle$ and $\langle \Pi_c^\ell \rangle$, respectively, all normalized by the energy dissipation rate $\varepsilon$. (*b*) Terms $\langle \Pi_S^\ell \rangle$, $\langle \Pi_\Omega^\ell \rangle$ and $\langle \Pi_c^\ell \rangle$ normalized by their sum $\langle \Pi^\ell \rangle$, together with data extracted from figure 3 of Johnson (2020) for comparison.

but normalized by the sum $\langle \Pi^\ell \rangle = \langle \Pi_S^\ell \rangle + \langle \Pi_\Omega^\ell \rangle + \langle \Pi_c^\ell \rangle$. Our results compare well with the data extracted from figure 3 of Johnson (2020). The very small differnces might be due to the different Reynolds numbers ($R_\lambda = 302$ in our work and 400 in Johnson (2020)).

Figure 2 shows various terms as functions of $\theta$ for fixed $\ell = 100\eta \approx 0.33 L_E$, where $L_E$ denotes the integral length scale given by $L_E \equiv (\pi/2\langle u_x^2 \rangle) \int_0^\infty E(k) k^{-1} dk$, where $u_x$ is the component of $x$ direction of the velocity. In figure 2(*a*), the red, blue and black lines refer to $I_1(\theta)$, $I_2(\theta)$ and $I_4(\theta)$, respectively. We see that $I_4(\theta)$ is indeed always positive in the range $0 \le \theta \le \ell^2$, as discussed in § 3, which ensures $\langle \Pi_S^\ell \rangle > \langle \Pi_\Omega^\ell \rangle$.

Note that in figure 2 the $I_4(\theta)$ curve is nearly independent of $\theta$, with a very slight decrease when $\theta/\eta^2 \lesssim 10^3$, which turns out to have interesting dynamic consequences. Johnson (2020) decomposed $\Pi_S^\ell$ and $\Pi_\Omega^\ell$ into local and non-local parts: $\Pi_S^\ell = \Pi_{l,S}^\ell + \Pi_{nl,S}^\ell$ and $\Pi_\Omega^\ell = \Pi_{l,\Omega}^\ell + \Pi_{nl,\Omega}^\ell$, where $\Pi_{l,S}^\ell \equiv -\bar{S}_{ik}^\ell \bar{S}_{kj}^\ell \bar{S}_{ji}^\ell \ell^2$ and $\Pi_{l,\Omega}^\ell \equiv \bar{\Omega}_{ik}^\ell \bar{S}_{kj}^\ell \bar{\Omega}_{ji}^\ell \ell^2$. The DNS results show that $\langle \Pi_{nl,S}^\ell \rangle$ is very close to $\langle \Pi_{nl,\Omega}^\ell \rangle$. Since $\langle \Pi_{l,S}^\ell \rangle = -\langle \bar{S}_{ik}^\ell \bar{S}_{kj}^\ell \bar{S}_{ji}^\ell \rangle \ell^2 = I_1(\ell^2)\ell^2$, this means that the local contribution $\langle \Pi_S^\ell \rangle$ simply equals the area of the

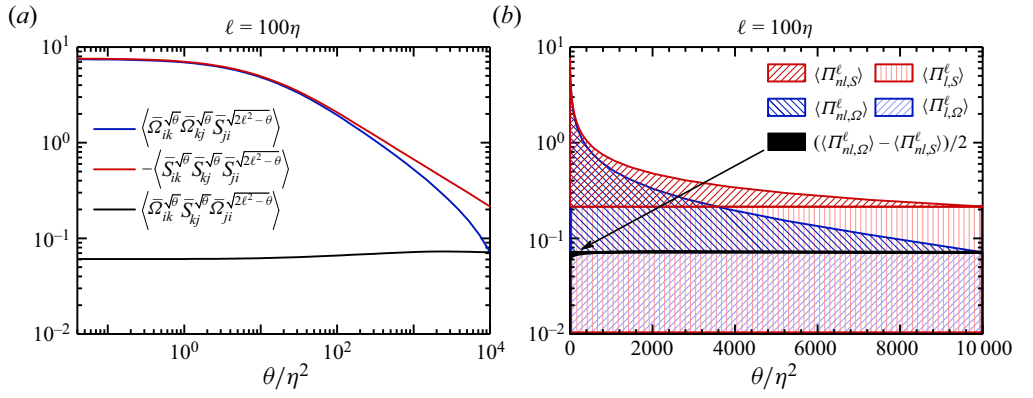


Figure 2. (*a*) Log–log plot of the DNS results for $I_1(\theta) \equiv -\langle \bar{S}_{ik}^{\sqrt{\theta}} \bar{S}_{kj}^{\sqrt{\theta}} \bar{S}_{ji}^{\sqrt{2\ell^2-\theta}} \rangle$, $I_2(\theta) \equiv \langle \bar{\Omega}_{ik}^{\sqrt{\theta}} \bar{\Omega}_{kj}^{\sqrt{\theta}} \bar{S}_{ji}^{\sqrt{2\ell^2-\theta}} \rangle$ and $I_4(\theta) \equiv \langle \bar{\Omega}_{ik}^{\sqrt{\theta}} \bar{S}_{kj}^{\sqrt{\theta}} \bar{\Omega}_{ji}^{\sqrt{2\ell^2-\theta}} \rangle$. (*b*) Same data as (*a*) but in a semi-log plot, with indications for the correspondence between several flux terms and the area of regions in the plot. The red shaded curved triangle, blue shaded curved triangle, red shaded rectangle, blue shaded rectangle and black area correspond to $\langle \Pi^\ell_{nl,S}\rangle$, $\langle \Pi^\ell_{nl,\Omega}\rangle$, $\langle \Pi^\ell_{l,S}\rangle$, $\langle \Pi^\ell_{l,\Omega}\rangle$ and $(\langle \Pi^\ell_{nl,\Omega}\rangle - \langle \Pi^\ell_{nl,S}\rangle)/2$, respectively.

red rectangle shown in figure 2(*b*). Similarly, $\langle \Pi^\ell_{l,\Omega}\rangle = -\langle \bar{\Omega}^\ell_{ik} \bar{S}^\ell_{kj} \bar{\Omega}^\ell_{ji}\rangle \ell^2 = I_2(\ell^2)\ell^2$ and corresponds to the area of the blue rectangle. The non-local contributions $\langle \Pi^\ell_{nl,S}\rangle$ and $\langle \Pi^\ell_{nl,\Omega}\rangle$ correspond to the areas of the red and blue curved triangles. The difference between $\langle \Pi^\ell_{nl,S}\rangle$ and $\langle \Pi^\ell_{nl,\Omega}\rangle$ is

$$\begin{aligned} \Pi^\ell_{nl,S} - \Pi^\ell_{nl,\Omega} &= (\Pi^\ell_S - \Pi^\ell_{l,S}) - (\Pi^\ell_\Omega - \Pi^\ell_{l,\Omega}) = (\Pi^\ell_S - \Pi^\ell_\Omega) - (\Pi^\ell_{l,S} - \Pi^\ell_{l,\Omega}) \\ &= 2\int_0^{\ell^2} I_4(\theta)\,\mathrm{d}\theta - \ell^2[I_1(\ell^2) - I_2(\ell^2)] \\ &\approx \ell^2[2I_4(\ell^2) - I_1(\ell^2) + I_2(\ell^2)] = 0, \end{aligned} \tag{4.1}$$

in which we used $I_4(\theta) \approx \text{const.} \approx I_4(\ell^2)$ and the identity (3.12).

In figure 2, the other two terms, $I_1(\theta)$ and $I_2(\theta)$, grow rapidly as $\theta$ decreases towards 0, and at $\theta = 0$, $I_1(0) \approx I_2(0) \gg I_4(0)$. To better understand this behaviour, we notice that for the isotropic case, (3.13) simplifies to $I_4(0) = \int_0^\infty \mathrm{d}r 4\pi r^2 G_4(r) \mathscr{G}^{\sqrt{2}\ell}(r)$, where $G_4(r) = \langle \Omega_{ik}(0) S_{kj}(0) \Omega_{ji}(r)\rangle$, and similarly, $I_1(0) = \int_0^\infty \mathrm{d}r 4\pi r^2 G_1(r) \mathscr{G}^{\sqrt{2}\ell}(r)$ and $I_2(0) = \int_0^\infty \mathrm{d}r 4\pi r^2 G_2(r) \mathscr{G}^{\sqrt{2}\ell}(r)$, with $G_1(r) \equiv -\langle S_{ik}(0) S_{kj}(0) S_{ji}(r)\rangle$ and $G_2(r) \equiv \langle \Omega_{ik}(0) \Omega_{kj}(0) S_{ji}(r)\rangle$. In figure 3(*a*) we plot $G_1$, $G_2$ and $G_4$ as functions of $r$, normalized by their values at $r = 0$. One can see that as $r$ increases, $G_4(r)$ decreases to 0 much faster than $G_1$ and $G_2$, which results in $I_4(0) \ll I_1(0)$ and $I_2(0)$. In figure 3(*b*) we show the filtered version of $G$'s in the HIT case, i.e. $G_1^{\sqrt{\theta}}(r) \equiv -\langle \bar{S}_{ik}^{\sqrt{\theta}}(0) \bar{S}_{kj}^{\sqrt{\theta}}(0) \bar{S}_{ji}^{\sqrt{\theta}}(r)\rangle$, $G_2^{\sqrt{\theta}}(r) \equiv \langle \bar{\Omega}_{ik}^{\sqrt{\theta}}(0) \bar{\Omega}_{kj}^{\sqrt{\theta}}(0) \bar{S}_{ji}^{\sqrt{\theta}}(r)\rangle$ and $G_4^{\sqrt{\theta}}(r) \equiv \langle \bar{\Omega}_{ik}^{\sqrt{\theta}}(0) \bar{S}_{kj}^{\sqrt{\theta}}(0) \bar{\Omega}_{ji}^{\sqrt{\theta}}(r)\rangle$. Those curves are qualitatively similar to those in figure 3(*a*); therefore, we still have $I_4(0) \ll I_1(0)$ and $I_2(0)$. In figures 3(*a*) and 3(*b*), the curves representing $G_1(r)$ and $G_1^{\sqrt{\theta}}(r)$ appear to be below those representing $G_2(r)$ and $G_2^{\sqrt{\theta}}(r)$ respectively and thus might raise the question as to whether indeed $I_1(\theta) > I_2(\theta)$. This confusion is due to the fact that $G_i(r)$ shown

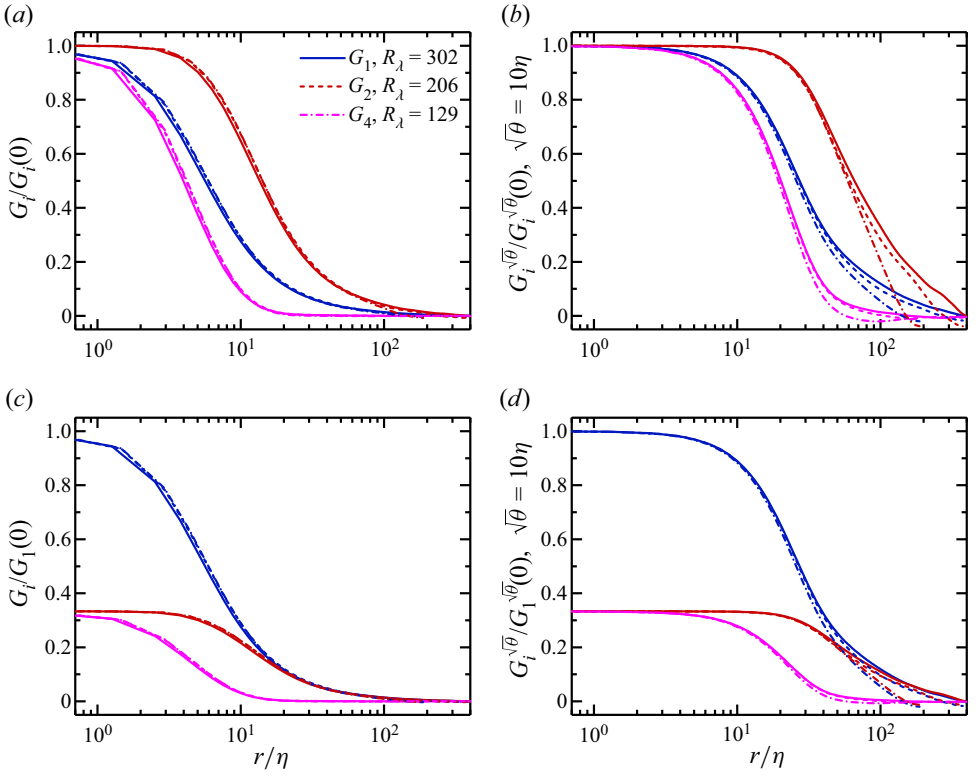


Figure 3. (*a*) The DNS results for $G_1(r)/G_1(0)$ (blue lines), $G_2(r)/G_2(0)$ (red lines) and $G_4(r)/G_4(0)$ (magenta lines), with solid lines for $R_\lambda = 302$, dashed lines for $R_\lambda = 206$ and dot-dashed lines for $R_\lambda = 129$. (*b*) The DNS results for $G_1^{\sqrt{\theta}}(r)/G_1^{\sqrt{\theta}}(0)$, $G_2^{\sqrt{\theta}}(r)/G_2^{\sqrt{\theta}}(0)$ and $G_4^{\sqrt{\theta}}(r)/G_4^{\sqrt{\theta}}(0)$, the line designations being the same as in (*a*). (*c*) Same as (*a*) but all curves are normalized by $G_1(0)$. (*d*) Same as (*b*) but all curves are normalized by $G_1^{\sqrt{\theta}}(0)$.

in figure 3(*a*) and 3(*b*) were normalized by their corresponding values at $r = 0$ and $G_i(0)$ differ in magnitude. In figures 3(*c*) and 3(*d*), the values of $G_i$ are plotted with non-dimensionalization by $G_1(0)$ or $G_1^{\sqrt{\theta}}(0)$, from which it is clearly seen that $G_1(r)$ and $G_1^{\sqrt{\theta}}(r)$ are above $G_2(r)$ and $G_2^{\sqrt{\theta}}(r)$ respectively. Thus we have $I_1(\theta) \gtrsim I_2(\theta) \gg I_4(\theta) > 0$, for $0 \leq \theta \leq \ell^2$. In addition, we notice that the proof of (3.14) could also be applied to $G_1^{\sqrt{\theta}}$ and $G_2^{\sqrt{\theta}}$; thus all the $G$ curves should cross zero once and this is consistent with figure 3, although the negative values are minuscule and hard to see from the figure.

Finally, we notice that the numerical results of Johnson (2020) show that the magnitudes of SSA and VS are $\langle \Pi_S^\ell \rangle : \langle \Pi_\Omega^\ell \rangle \approx 5 : 3$. Based on a simple K41-type scaling argument, our approach developed here leads to an approximate estimate of this ratio, namely $\langle \Pi_S^\ell \rangle : \langle \Pi_\Omega^\ell \rangle \approx 9 : 5$, as shown in detail in the Appendix. The quantitative deviation of the model prediction from the DNS results indicates that the simple scaling analysis is not enough to describe the third-order moments of filtered velocity gradient.

## 5. Concluding remarks

In summary, we showed that in the filtered energy equation, the three contributions to the mean inter-scale energy transfer from SSA, VS and the correlation between strain

and vorticity can all be expressed as integrals of third-order moments of filtered velocity gradients associated with two different filter sizes (equation (3.10)). With the help of that representation, and a relation involving third-order moments of filtered velocity gradients in homogeneous flows (equation (3.11)), we explained the observation that SSA dominates VS in kinetic energy transfer (Johnson 2020). Although the analytical results were compared with DNS of HIT, the derivation presented in this work is not restricted to HIT and could be applied to any homogeneous flows. Furthermore, the homogeneity constraint (equation (3.11)) provides an explanation to the observed nearly equal contributions from multi-scale strain amplification and VS (see figure 2*b*). We notice that those third-order moments of filtered velocity gradient (i.e. $I_1$ to $I_4$ in the text) could not be described by simple scaling analysis. Thus in the future it would be interesting to quantitatively investigate their properties, especially their roles in inter-scale energy transfer. Also, DNS of homogeneous but anisotropic turbulence could be used to verify the theoretical arguments in this work.

**Acknowledgements.** We thank Professors L.B. Pan and A. Pumir for helpful discussions.

**Funding.** This research is supported by the Natural Science Foundation of China (NSFC) Basic Science Center Program for 'Multiscale Problems in Nonlinear Mechanics' (no. 11988102) and also NSFC grants 91852104 and 12202452.

**Declaration of interests.** The authors report no conflict of interest.

**Author ORCIDs.**
P.-F. Yang https://orcid.org/0000-0003-1949-500X;
Z.D. Zhou https://orcid.org/0000-0002-7505-5626;
H. Xu https://orcid.org/0000-0002-2863-7658;
G.W. He https://orcid.org/0000-0003-4738-0816.

## Appendix

In this appendix we discuss the ratio between magnitudes of SSA and VS based on a K41-type scaling argument. As discussed in Johnson (2020, 2021), the energy transfer due to SSA and VS, $\Pi_S^\ell$ and $\Pi_\Omega^\ell$, can be decomposed into local and non-local parts: $\Pi_S^\ell = \Pi_{l,S}^\ell + \Pi_{nl,S}^\ell$ and $\Pi_\Omega^\ell = \Pi_{l,\Omega}^\ell + \Pi_{nl,\Omega}^\ell$. Then the Betchov relation leads to $\langle \Pi_{l,S}^\ell \rangle : \langle \Pi_{l,\Omega}^\ell \rangle = 3:1$, and numerical evidence shows that $\langle \Pi_{nl,S}^\ell \rangle : \langle \Pi_{nl,\Omega}^\ell \rangle \approx 1:1$, as discussed in § 4. With these results, to understand the observed ratio $\langle \Pi_S^\ell \rangle : \langle \Pi_\Omega^\ell \rangle \approx 5:3$, one only needs to discuss the ratio between the local contribution and the total VS, that is, $\langle \Pi_{l,\Omega}^\ell \rangle : \langle \Pi_\Omega^\ell \rangle$. As given by (3.7), $\langle \Pi_\Omega^\ell \rangle = \int_0^{\ell^2} \mathrm{d}\theta \langle \bar{\Omega}_{ik}^{\sqrt{\theta}} \bar{\Omega}_{kj}^{\sqrt{\theta}} \bar{S}_{ji}^{\sqrt{2\ell^2-\theta}} \rangle = \int_0^{\ell^2} \mathrm{d}\theta I_2(\theta)$. Thus a naive, K41-type scaling argument leads to

$$I_2(\theta) \sim \left( \frac{\bar{u}^{\sqrt{\theta}}}{\sqrt{\theta}} \right)^2 \frac{\bar{u}^{\sqrt{2\ell^2-\theta}}}{\sqrt{2\ell^2-\theta}} \sim \varepsilon \theta^{-2/3} (2\ell^2 - \theta)^{-1/3}, \tag{A1}$$

which suggests that one could try a simple form as

$$I_2(\theta) = \begin{cases} C_{I2} \varepsilon \theta^{-2/3} (2\ell^2 - \theta)^{-1/3} & (\eta^2 < \theta \le \ell^2), \\ C_{I2} \varepsilon \eta^{-4/3} (2\ell^2 - \eta^2)^{-1/3} & (0 \le \theta \le \eta^2), \end{cases} \tag{A2}$$

where $C_{I2}$ is a dimensionless coefficient that might depend on $\ell/\eta$, but independent of $\theta$. The predicted behaviour of $I_2(\theta)$ from this model is shown in figure 4, together with the

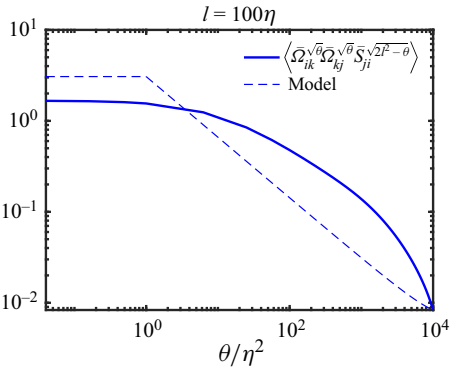


Figure 4. Log–log plot of the DNS results for $I_2(\theta) \equiv \langle \bar{\Omega}_{ik}^{\sqrt{\theta}} \bar{\Omega}_{kj}^{\sqrt{\theta}} \bar{S}_{ji}^{\sqrt{2\ell^2-\theta}} \rangle$ and the prediction of the model given by (A2).

DNS result. As shown in the main text, the local contribution to VS is

$$\langle \Pi_{l,\Omega}^{\ell} \rangle = I_2(\ell^2)\ell^2 = C_{I2}\,\varepsilon \ell^{-4/3}(2\ell^2 - \ell^2)^{-1/3}\ell^2 = C_{I2}\,\varepsilon. \tag{A3}$$

The total VS is

$$\begin{aligned}\langle \Pi_{\Omega}^{\ell} \rangle &= \int_0^{\ell^2} \mathrm{d}\theta I_2(\theta) = C_{I2}\,\varepsilon \int_{\eta^2}^{\ell^2} \theta^{-2/3}(2\ell^2 - \theta)^{-1/3}\,\mathrm{d}\theta + \eta^2 I_2(0) \\ &= C_{I2}\,\varepsilon \left[ \frac{1}{2}\ln(t^2 - t + 1) + \sqrt{3}\mathrm{atan}\left(\frac{2t-1}{\sqrt{3}}\right) - \ln(t+1) \right]_1^{t_\ell} + 2^{-1/3} C_{I2}\,\varepsilon \left(\frac{\eta}{\ell}\right)^{2/3},\end{aligned} \tag{A4}$$

where $t_\ell = (2(\ell/\eta)^2 - 1)^{1/3}$. For the usual filter size in the inertial range, $\ell \gg \eta$, we have $t_\ell \gg 1$. In that case, the result above can be simplified to

$$\langle \Pi_{\Omega}^{\ell} \rangle \approx \left( \frac{\pi}{\sqrt{3}} + \ln 2 \right) C_{I2}\varepsilon. \tag{A5}$$

Comparing (A3) and (A5), we see that

$$\langle \Pi_{l,\Omega}^{\ell} \rangle : \langle \Pi_{\Omega}^{\ell} \rangle \approx 1 : \left( \frac{\pi}{\sqrt{3}} + \ln 2 \right) \approx 1 : 2.5, \tag{A6}$$

which gives an estimate of the ratio between SSA and VS as

$$\begin{aligned}\langle \Pi_{S}^{\ell} \rangle : \langle \Pi_{\Omega}^{\ell} \rangle &= (\langle \Pi_{l,S}^{\ell} \rangle + \langle \Pi_{nl,S}^{\ell} \rangle) : \langle \Pi_{\Omega}^{\ell} \rangle \approx (3\langle \Pi_{l,\Omega}^{\ell} \rangle + \langle \Pi_{nl,\Omega}^{\ell} \rangle) : \langle \Pi_{\Omega}^{\ell} \rangle \\ &= (2\langle \Pi_{l,\Omega}^{\ell} \rangle + \langle \Pi_{\Omega}^{\ell} \rangle) : \langle \Pi_{\Omega}^{\ell} \rangle \approx (2 + 2.5) : 2.5 = 9 : 5,\end{aligned} \tag{A7}$$

which is not too far from the observed ratio of 5 : 3. Possible reasons for the deviation might include (i) the alignment between the filtered strain $\bar{S}_{ij}^{\ell_2}$ and vorticity $\bar{\omega}_i^{\ell_1}$ might be scale-dependent and especially on the ratio $\ell_2/\ell_1$; and (ii) the filtered velocity gradient $\bar{A}_{ij}^{\ell}$ contains information at length scales other than $\ell$, and thus the simple scaling argument fails to catch its quantitative behaviour.

## References


Ballouz, J.G. & Ouellette, N.T. 2018 Tensor geometry in the turbulent cascade. *J. Fluid Mech.* **835**, 1048–1064.

Ballouz, J.G. & Ouellette, N.T. 2020 Geometric constraints on energy transfer in the turbulent cascade. *Phys. Rev. Fluids* **5**, 034603.

Betchov, R. 1956 An inequality concerning the production of vorticity in isotropic turbulence. *J. Fluid Mech.* **1**, 497–504.

Borue, V. & Orszag, S.A. 1998 Local energy flux and subgrid-scale statistics in three-dimensional turbulence. *J. Fluid Mech.* **366**, 1–31.

van der Bos, F., Tao, B., Meneveau, C. & Katz, J. 2002 Effects of small-scale turbulent motions on the filtered velocity gradient tensor as deduced from holographic particle image velocimetry measurements. *Phys. Fluids* **14** (7), 2456–2474.

Buzzicotti, M., Linkmann, M., Aluie, H., Biferale, L., Brasseur, J. & Meneveau, C. 2018 Effect of filter type on the statistics of energy transfer between resolved and subfilter scales from a-priori analysis of direct numerical simulations of isotropic turbulence. *J. Turbul.* **19** (2), 167–197.

Carbone, M. & Bragg, A.D. 2020 Is vortex stretching the main cause of the turbulent energy cascade? *J. Fluid Mech.* **883**, R2.

Danish, M. & Meneveau, C. 2018 Multiscale analysis of the invariants of the velocity gradient tensor in isotropic turbulence. *Phys. Rev. Fluids* **3**, 044604.

Davidson, P.A. 2015 *Turbulence: An Introduction for Scientists and Engineers*, 2nd edn. Oxford Press.

Doan, N.A.K., Swaminathan, N., Davidson, P.A. & Tanahashi, M. 2018 Scale locality of the energy cascade using real space quantities. *Phys. Rev. Fluids* **3**, 084601.

Dong, S., Huang, Y., Yuan, X. & Lozano-Durán, A. 2020 The coherent structure of the kinetic energy transfer in shear turbulence. *J. Fluid Mech.* **892**, A22.

Eyink, G. 1995 Local energy flux and the refined similarity hypothesis. *J. Stat. Phys.* **78**, 335–351.

Eyink, G. 2006 Multi-scale gradient expansion of the turbulent stress tensor. *J. Fluid Mech.* **549**, 159–190.

Fiscaletti, D., Attili, A., Bisetti, F. & Elsinga, G.E. 2016*a* Scale interactions in a mixing layer - the role of the large-scale gradients. *J. Fluid Mech.* **791**, 154–173.

Fiscaletti, D., Elsinga, G.E., Attili, A., Bisetti, F. & Buxton, O.R.H. 2016*b* Scale dependence of the alignment between strain rate and rotation in turbulent shear flow. *Phy. Rev. Fluids* **1**, 064405.

Frisch, U. 1995 *Turbulence: The Legacy of A. N. Kolmogorov*. Cambridge University Press.

He, G.W., Jin, G.D. & Yang, Y. 2017 Space-time correlations and dynamic coupling in turbulent flows. *Annu. Rev. Fluid Mech.* **49**, 51–70.

Higgins, C.W., Parlange, M.B. & Meneveau, C. 2003 Alignment trends of velocity gradients and subgrid-scale fluxes in the turbulent atmospheric boundary layer. *Boundary-Layer Meteorol.* **109**, 59–83.

Johnson, P.L. 2020 Energy transfer from large to small scales in turbulence by multiscale nonlinear strain and vorticity interactions. *Phys. Rev. Lett.* **124**, 104501.

Johnson, P.L. 2021 On the role of vorticity stretching and strain self-amplification in the turbulence energy cascade. *J. Fluid Mech.* **922**, A3.

Kolmogorov, A.N. 1941*a* Dissipation of energy in locally isotropic turbulence. *Dokl. Akad. Nauk SSSR* **32**, 16–18.

Kolmogorov, A.N. 1941*b* The local structure of turbulence in incompressible viscous fluid for very large Reynolds numbers. *Dokl. Akad. Nauk SSSR* **30**, 299–303.

Leung, T., Swaminathan, N. & DaVidson, P.A. 2012 Geometry and interaction of structures in homogeneous isotropic turbulence. *J. Fluid Mech.* **710**, 453–481.

Lozano-Durán, A., Holzner, M. & Jiménez, J. 2016 Multiscale analysis of the topological invariants in the logarithmic region of turbulent channels at a friction Reynolds number of 932. *J. Fluid Mech.* **803**, 356–394.

Meneveau, C. 2011 Lagrangian dynamics and models of the velocity gradient tensor in turbulent flows. *Annu. Rev. Fluid Mech.* **43**, 219–245.

Meneveau, C. & Katz, J. 2000 Scale-invariance and turbulence models for large-eddy simulation. *Annu. Rev. Fluid Mech.* **32**, 1–32.

Pope, S.B. 2000 *Turbulent Flows*. Cambridge University Press.

Pullin, D.I. & Saffman, P.G. 1998 Vortex dynamics in turbulence. *Annu. Rev. Fluid Mech.* **30**, 31–51.

Richardson, L.F. 1922 *Weather Prediction by Numerical Processes*. Cambridge University Press.

Tao, B., Katz, J. & Meneveau, C. 2000 Geometry and scale relationships in high Reynolds number turbulence determined from three-dimensional holographic velocimetry. *Phys. Fluids* **12**, 941–944.

Tao, B., Katz, J. & Meneveau, C. 2002 Statistical geometry of subgrid-scale stresses determined from holographic particle image velocimetry measurements. *J. Fluid Mech.* **457**, 35–78.

TAYLOR, G.I. 1937 The statistical theory of isotropic turbulence. *J. Aeronaut. Sci.* **4**, 311–315.
TAYLOR, G.I. 1938 Production and dissipation of vorticity in a turbulent fluid. *Proc. R. Soc. Lond.* A **164**, 15–23.
TENNEKES, H. & LUMLEY, J.L. 1972 *A First Course in Turbulence*. MIT Press.
TRITTON, D.J. 1988 *Physical Fluid Dynamics*, 2nd edn. Oxford University Press.
TSINOBER, A. 2009 *An Informal Conceptual Introduction to Turbulence*. Springer.
VELA-MARTÍN, A. & JIMÉNEZ, J. 2021 Entropy, irreversibility and cascades in the inertial range of isotropic turbulence. *J. Fluid Mech.* **915**, A36.
YANG, P.-F., FANG, J., FANG, L., PUMIR, A. & XU, H. 2022 Low-order moments of the velocity gradient in homogeneous compressible turbulence. *J. Fluid Mech.* **947**, R1.
YANG, P.-F., PUMIR, A. & XU, H. 2020 Dynamics and invariants of the perceived velocity gradient tensor in homogeneous and isotropic turbulence. *J. Fluid Mech.* **897**, A9.
ZHOU, Z.D., HE, G.W., WANG, S.Z. & JIN, G.D. 2019 Subgrid-scale model for large-eddy simulation of isotropic turbulent flows using an artificial neural network. *Comput. Fluids* **195**, 104319.
ZHOU, Z.D., WANG, S.Z. & JIN, G.D. 2018 A structural subgrid-scale model for relative dispersion in large-eddy simulation of isotropic turbulent flows by coupling kinematic simulation with approximate deconvolution method. *Phys. Fluids* **30**, 105110.